ELSEVIER

Journal of Chromatography A, 753 (1996) 177–190

JOURNAL OF CHROMATOGRAPHY A

Packings of an unidimensional regular pore structure as model packings in size-exclusion and inverse size-exclusion chromatography

A. Kurganov*, K. Unger, T. Issaeva

Institut für Anorganische Chemie und Analytische Chemie, Johannes Gutenberg-Universität, J. Becher Weg 24, 55099 Mainz, Germany

Received 31 January 1996; revised 6 June 1996; accepted 6 June 1996

Abstract

Using porous aluminas and aluminosilicates with a regular and well-defined pore structure an attempt was made to correlate the SEC data of polystyrenes with established theoretical models. The pore structure of the two types of packings was extensively characterized by means of transmission and scanning electron microscopy, nitrogen sorption and mercury porosimetry. The SEC distribution coefficients measured experimentally were correlated with the distribution coefficients calculated from the theoretical models for flexible polymers. A good correlation was observed for the packing of the simplest pore morphology, but remarkable deviations appeared for the materials with a more complex pore structure. The results of correlation were considered in terms of their applicability to estimate pore morphology from SEC measurements.

Keywords: Polymers; Stationary phases, LC; Adsorbents; Membranes; Pore structure

1. Introduction

Size-exclusion chromatography (SEC) is a chromatographic technique widely used for the separation of polymers, the assessment of the molecular mass distribution of polymers and for the characterization of the porosity of porous materials [1]. In the latter application SEC is designated as inverse size-exclusion chromatography (ISEC) or macromolecular porosimetry [2]. A number of theoretical models have been developed to describe the experimental results in SEC [3–18] and in ISEC [19–23]. These theories are often non-compatible with each other because of the widely divergent assumptions made. Nevertheless, an apparent fairly good agreement was found between the experimental data and the predictions made by the widely divergent models. Hussain et al. [18] have stated that this is at least in part a result of the mathematical functions used in these models. On the other hand, comparing the experimental data with theoretical predictions minor corrections are often needed to bring the theory and the experiment in an excellent coincidence. It appears that not only mathematical functions used but other fundamental parameters as well should be minutely considered to explain why widely divergent models can well describe the same set of the experimental data.

*Corresponding author.

0021-9673/96/$15.00
PII S0021-9673(96)00552-3

Any of the theoretical models for SEC and ISEC tries to ascertain the relation between the two fundamental characteristics, i.e. the dimension of a polymeric solute and the porosity of a porous adsorbent. Both characteristics are of statistical nature.

There are at least three frequently used, different means to define the dimension of a polymeric molecule in solution:

(a) the Stokes radius, r_S

$$r_S = \frac{kT}{6\pi\eta_o D} \quad (1)$$

where k, T, η_o and D are the Boltzmann constant, the absolute temperature, the solvent viscosity and the translational diffusion coefficient, respectively.

(b) the hydrodynamic (viscosimetric) radius, r_η:

$$r_\eta = \left[\frac{3[\eta]\bar{M}_w}{10\pi N_a} \right] \quad (2)$$

where $[\eta]$ and N_a are the intrinsic viscosity and Avogadro's number, respectively.

(c) the radius of gyration, r_g:

the weight average value of the radius of gyration r_g can be found from the unperturbated mean-square end-to-end distance r_o of polymeric molecule. Values of $r_o/M_w^{0.5}$ are tabulated in [33].

All three types of radii have been applied in modeling SEC and ISEC. The Stokes radius was almost exclusively used in modeling the separation of biopolymers (proteins, peptides etc.,). In SEC of synthetic polymers mainly the hydrodynamic radius is applied, particularly in context with the universal calibration curve (UCC). The radius of gyration was widely applied in ISEC and in some theoretical models of SEC. The choice between one of these parameters is probably less critical in practical applications of SEC, where an experimentally measured calibration curve is used later to calculate the molecular mass of an unknown sample. However, in theoretical considerations of SEC and particularly in ISEC, the type of radius used is of primary importance, because e.g., the value of the mean pore size and the pore size distribution calculated in ISEC are directly dependent on the radius of polymeric molecule used in the calculations. Recently, Monte-Carlo simulations have been performed by Degoulet et al. [29] to estimate the relation between the chromatographic radius, r_C, i.e., the radius of a polymeric solute calculated from chromatographic data, and the radii r_S, r_η and r_g. The results indicate that there is no coincidence between r_C and the other radii and the ratios of r_C/r_g, r_C/r_S and r_C/r_η were depending on the flexibility of the polymeric chains and the pore geometry (slits, cylinders, spheres).

The simulations by Degoulet et al. [29] recalled the pore shape of a porous adsorbent as an important parameter in SEC. This is not suprising, because already one of the first theories in SEC by Cassassa et al. [8] proposed a strong effect of the pore shape on the calibration curve:

$$K = (1 - r/R)^\lambda \quad (3)$$

where K is the distribution coefficient equivalent to the ratio of the solute concentration in the pore and in the bulk solvent, respectively, r is the radius of the sphere equivalent to the radius of the polymeric molecule; R is the pore radius and λ is a coefficient accounting for the pore geometry: $\lambda = 1$ for a slit pore, $\lambda = 2$ for a cylindrical pore of circular or of square cross-section, $\lambda = 3$ for a spherical or a cubic pore.

Many of the later developed models simply approximate the porous structure of real adsorbents by an array of uniform cylindrical pores. In reality, typical adsorbents such as controlled pore glass [24], porous silicas [12,25] and polymers [26,27] show a pore structure which resembles an array of partially fused small spherical or irregular particles with a complex pore geometry. In addition, the width of the pore size distributions of real packings can also affect the results of a comparison between the experiment and the theory. The latter parameter was taken into account in some models [11,12,18,28], but again assuming a cylindrical shape of the pores. It is worth to note that the mean pore size and the pore size distribution of a rigid chromatographic packing are commonly measured by low temperature nitrogen sorption or by mercury porosimetry. Both of these methods assume a cylindrical pore shape of the packing as well. Thus, the calculation of the mean pore radius and the pore size distribution gives only pore dimensions being equivalent to a cylindrical pore irrespective of the real pore shapes. The inconsistency between the values provided by conventional methods (nitrogen sorption, mercury porosimetry)

and the values needed for SEC and ISEC can also affect a comparison between the theory and the experiment.

From the discussion above it is evident, that any comparison of the theoretical and the experimental data in SEC and ISEC requires an answer to the following two questions:

1. What type of molecular dimension of a polymeric solute approximates best the chromatographic radius of the polymer.
2. Can one obtain pore structural data from mercury porosimetry or low temperature nitrogen sorption applicable to both ISEC and SEC.

Using a packing of an ideal cylindrical pore geometry for SEC and ISEC measurements would fulfill best the desired conditions. However, such type of packing is not available.

Recently, porous adsorbents have been synthesized [31,32] which come very close to this demand. The material possess a regular pore structure with a fairly uniform pore width of approximately cylindrical pore shape and a rather narrow pore size distribution. A common feature of these packings is that they have an unidimensional pore structure, i.e., all pore channels are directed in one dimension and do not intersect. The pore structure characteristics of these packings were assessed by scanning and transmission electron microscopy, mercury porosimetry, nitrogen sorption and X-ray diffraction measurements. The aim of this study is to apply these new packings in SEC of polystyrenes and to compare the experimental calibration curves with theoretical calculations based on some current theories.

2. Experimental

2.1. Packings

Anatop membranes composed of transition aluminas and designated as MEM-200, MEM-100 and MEM-20 were a gift of Whatman (Banbury, UK). MEM-200 is a symmetrical porous alumina membrane with a nominal mean pore diameter of 200 nm (Fig. 1c). The thickness of the membrane is 60 μm. MEM-100 and MEM-20 are unsymmetrical

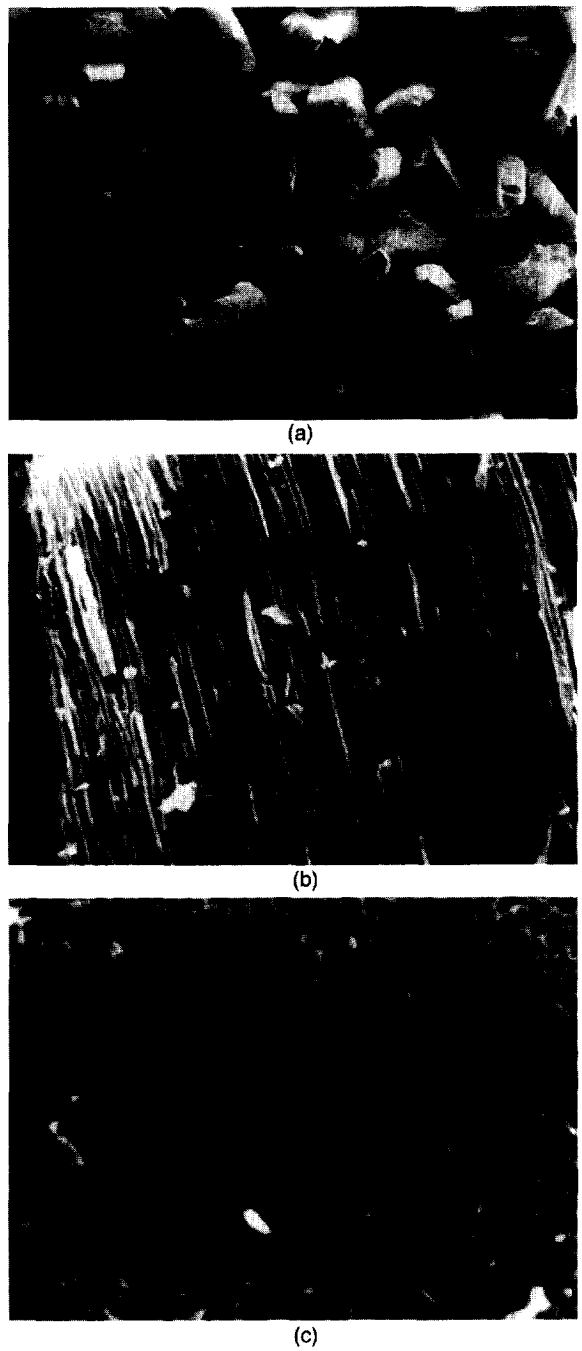

Fig. 1. Scanning electron microphotos of MEM-200 packing. (a) general view of particles; (b) cross-section of a particle; (c) pore opening.

porous alumina membranes consisting of two porous layers (Fig. 2a). The first layer has a thickness of 60 μm and a nominal pore diameter of 200 nm. The second layer of a ca. 1 μm thickness is deposited on the first layer. The mean pore diameter of the second layer is 100 nm for the MEM-100 material and 20 nm for the MEM-20 material.

The membranes were carefully crushed in a mortar to retain the particle thickness equal to the thickness of the membrane (Fig. 1a). The fraction of particles with a size range between 100 and 500 μm was separated by sedimentation in acetone. The shape of the particles is displayed in Fig. 1a.

The second type of packing under investigation was the MCM-41 (Mobile Composition of Material 41) [31]. MCM-41 is an amorphous aluminosilicate with an unidimensional regular pore shape. The primary particles possess a hexagonal array of uniform unidimensional channels with hexagonal pore shape. Synthesis of aluminosilicate MCM-41 was performed as described everywhere [31]. The structural characteristics of MCM-41 were assessed by the low temperature nitrogen sorption, low angle X-ray diffraction and from transmission electron microscopy (TEM) [32]. The characteristics of the pore structure of the MCM-41 sample used in the study are presented in Table 1. The as-synthesized material was crushed and fractionated by sedimentation in acetone. The final fraction obtained had a mean particle size of $d_p \sim 10$ μm. The value of d_p at 90% (10%) of the cumulative size distribution was $d_{p90} = 17$ μm ($d_{p10} = 6$ μm).

2.2. Packing of columns

In all experiments the column dimensions were kept constant at 250 mm length and 8 mm inner diameter. The membrane packings were dry-packed in the column, while MCM-41 was packed by the slurry technique using a suspension in acetone. The column characteristics are shown in Table 1.

2.3. Chromatographic equipment

All chromatographic experiments were performed using a chromatographic system composed of an analytical pump 655A (E. Merck, Darmstadt, Germany), a variable-wavelength UV detector 655A (E. Merck) and a Rheodyne injector 7125 (Reodyne,

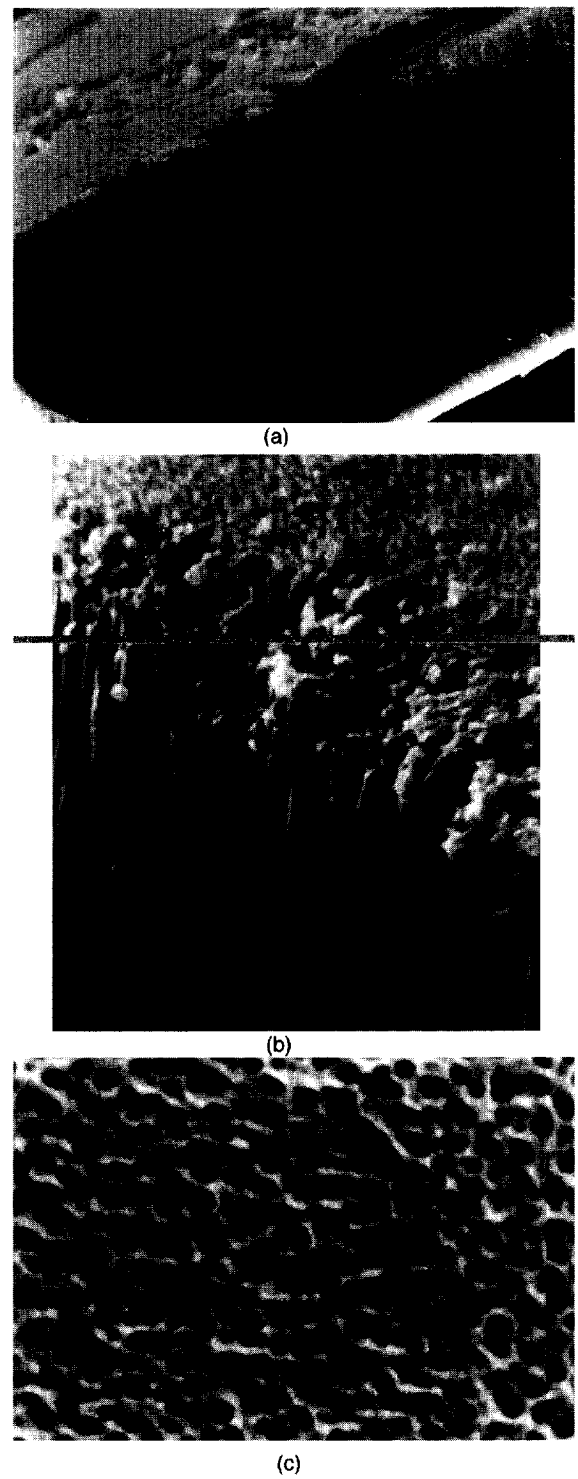

Fig. 2. Scanning electron microphotos of MEM-20 packing. (a) general view of a particle; (b) cross-section of a particle; (c) pore opening on the wide pore side.

Table 1
Characteristics of the packings and the columns[1] used in the study

Type of Packing[2]	Specific pore volume[3] (ml/g)	Specific surface area[3] (m^2/g)	Mean pore radius[3] (nm)	RSD-value of pore size distribution	Amount of packing in the column (g)	Intersitial volume[4] (ml)	Void volume[4] (ml)	Total column porosity[4]	Specific packing density[4] (g/ml)	Pore volume[4] (ml/g)
MEM-200	0.493	11.1	115	25.9	9.54	4.46	9.29	0.36	3.26	0.51
MEM-100	0.544	10.4	116	25.1	8.7	4.67	9.63	0.35	3.37	0.57
MEM-20	0.201	6.9	106;47[7]	9.7;8.4[7]	14.63	5.01	7.5	0.41	3.11	0.17
MCM-41	2.007 0.818[5]	62.3 756.3[5]	236 4.3[5]		3.18	ca. 7.5[6]	10.47	ca. 0.64[6]	1.836	0.936

[1] The same column of 243x8 mm in size was used for all experiments. The total geometrical volume was 12.21 ml.
[2] For the abbreviation see Section 2.1.
[3] Derived from mercury porosimetry.
[4] Derived from SEC.
[5] Derived from low temperature nitrogen sorption.
[6] Only approximated values could be determined, see Section 3.1.
[7] Bimodal pore size distribution.

Table 2
Weight-average molecular mass M_w and polydispersity M_w/M_n of polystyrene standards used in the study

M_w	M_w/M_n	M_w	M_w/M_n	M_w	M_w/M_n
580	1.23	9000	1.08	180 000	1.1
730	1.16	9770	1.05	233 000	1.15
800	1.30	11 800	1.08	390 000	1.1
920	1.07	39 000	1.05	500 000	1.1
1520	1.07	50 000	1.03	600 000	1.16
2200	1.06	55 000	1.02	770 000	1.1
2480	1.06	76 000	1.05	900 000	1.18
4050	1.05	85 000	1.05	1 800 000	1.2
4250	1.11	110 000	1.05	3 340 000	1.09

Palo Alto, CA, USA) equipped with 20-μl sample loop. All measurements were performed at room temperature. The "ChromStar LC 42" software, SCPA (Weyhe, Germany) was used to collect and to calculate the chromatographic data.

2.4. Characterization of packings

Scanning electron micrographs were obtained with a Zeiss DSM 962 microscope (Carl Zeiss, Oberkochen, Germany).

Nitrogen sorption measurements were performed on ASAP 2000 (Micromeritics, USA) at liquid nitrogen temperature using a standard protocol and the software implemented in the equipment.

Mercury porosimetry was carried on a Porosimeter 2000 (Carlo Erba, Italy), according to a standard procedure with a maximum pressure of 2000 bar. A mercury contact angle of 141.3° and the surface tension of 480 mNm^{-1} were used in the calculation of the pore size distribution.

X-Ray diffraction measurements were made with a diffractometer APD 15 (Philips, Eindhoven, Netherlands).

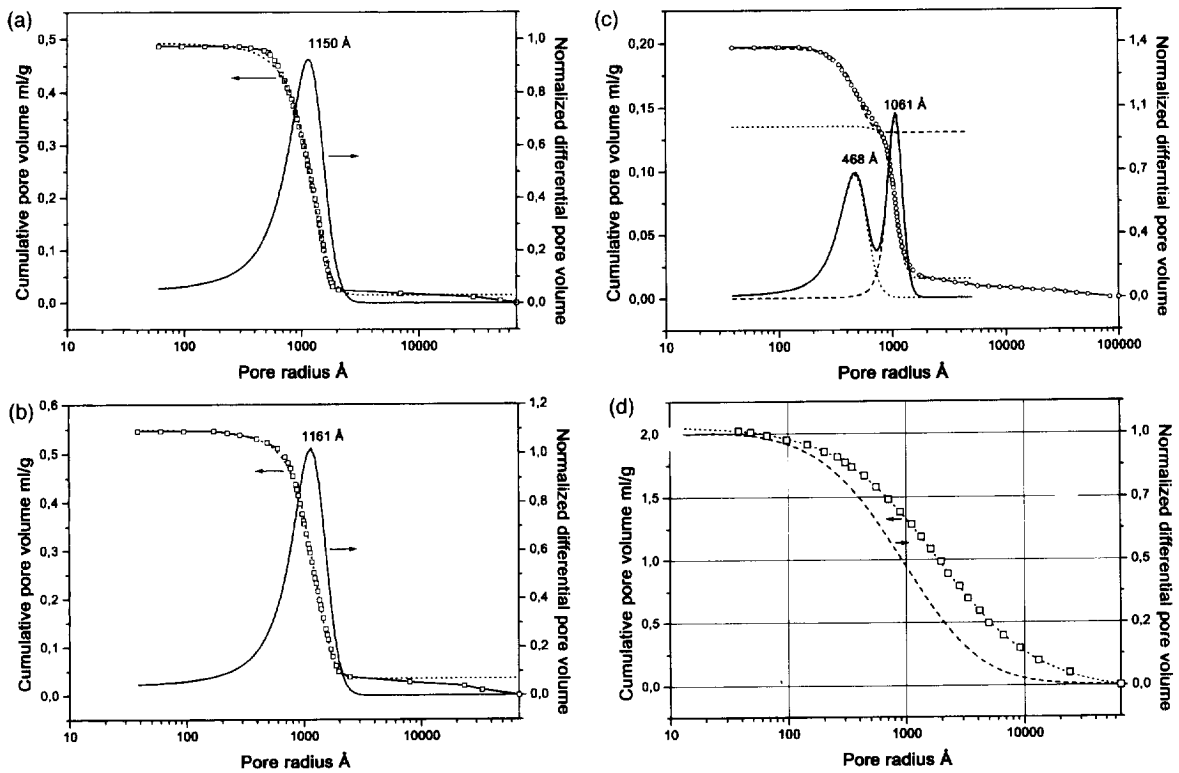

Fig. 3. Mercury intrusion curve and calculated pore size distribution of MEM- and MCM-packings. (a) MEM-200; (b) MEM-100; (c) MEM-20 and (d) MCM-41.

2.5. Chemicals

All solvents were of chromatographic grade and purchased from E. Merck. Polystyrene standards were purchased from Polymer Standards Service (Mainz, Germany) and from Polymer Laboratories (Essex, UK). The mean molecular mass (M_w) of polystyrenes and the polydispersity value (M_w/M_n) are given in Table 2.

(a) The Stokes radius of polystyrene molecules was calculated based on the relation between the diffusion coefficient D and M_w ($D=3.45\times10^{-4}M_w^{-0.564}$) reported in the literature [33] for the molecular mass range of polystyrenes between 20 and $1800\cdot10^3$ [33] and tetrahydrofuran as a solvent at 25°C:

$$r_S = 0.132M_w^{0.564} \quad (4)$$

(b) The hydrodynamic radius of polystyrene was evaluated from the coefficients of the Mark–Houwink equation for polystyrene in tetrahydrofuran at 25°C ($K=14\cdot10^{-3}$ and $\alpha=0.70$) [33]:

$$r_\eta = 0.130M_w^{0.566} \quad (5)$$

(c) The relation between r_g and M_w for polystyrene in any solvent is [33]:

$$r_g = 0.408\alpha r_o = \alpha 0.27M_w^{0.5} \quad (6)$$

where α is a coefficient accounting for long-range interactions in the polymeric molecule; α is equal to ζM_w^z, where usually $0\leq\zeta\leq1$ and $0\leq z\leq0.1$ are parameters accounting for the solvent–polymer interactions [17]. According to Van Kreveld and Van den Hoed [12] the following expression can be obtained for polystyrenes in tetrahydrofuran:

$$r_g = 0.139M_w^{0.588} \quad (7)$$

It can be easily seen from the Eqs. (4,5), that the Stokes radius r_s and the hydrodynamic radius r_η of polystyrenes are essentially equal under the experimental conditions used. The coincidence between r_S and r_η was also observed for some other polymers [15,30,34,35].

3. Results

3.1. Investigation of the pore structure of packings

The porosity of the membrane packings was investigated by means of mercury porosimetry (MEM-200, MEM-100 and MEM-20, Table 1) and by the low temperature nitrogen sorption (MEM-20, MCM-41, Table 1).

In accordance with the pore structure observed by means of SEM, the MEM-200 packing showed only one sharp step in the intrusion curve (Fig. 3a). The mean pore diameter of 230 nm calculated from the intrusion curve coincided fairly well with the nominal pore size of the membrane reported by the manufacturer.

The results of sorption measurements on MEM-20 were totally unexpected: the specific surface area of the MEM-20 packing was found to be of 3.5 m^2/g and the specific pore volume 0.009 ml/g only. The values are indicative for a non-porous adsorbent, whereas the SEM measurements clearly showed a porous material (Fig. 2b,c). The mercury porosimetry of the MEM-20 packing gave two steps in the intrusion curve (Fig. 3c) indicative for a bimodal pore size distribution. The first step corresponds to the pores of the mean radius of 47 nm, the second to pores of a mean radius of 106 nm. When one separates the specific pore volume of the small and the large pores at the inflection point of the intrusion curve (Fig. 3), the specific pore volume of the 47 nm pores calculates to 0.062 ml/g and that of 106 nm pores to 0.139 ml/g. The specific pore volume of the large pores of the MEM-20 material was only about 29% of the specific pore volume of the MEM-200 material. The strong reduction of the specific pore volume of the large pores of MEM-20 is rather unexpected. According to the information of the manufacturer the asymmetrical membranes MEM-20 and MEM-100 are synthesized on basis of symmetrical MEM-200 material. Therefore, the same porosity of the large pore size layer could be expected for all MEM-packings. A possible explanation of the observed difference might be that the pore structure of the first layer was changed during the deposition of the second layer or MEM-20 was prepared on the basis of MEM-200 membrane of lower porosity than

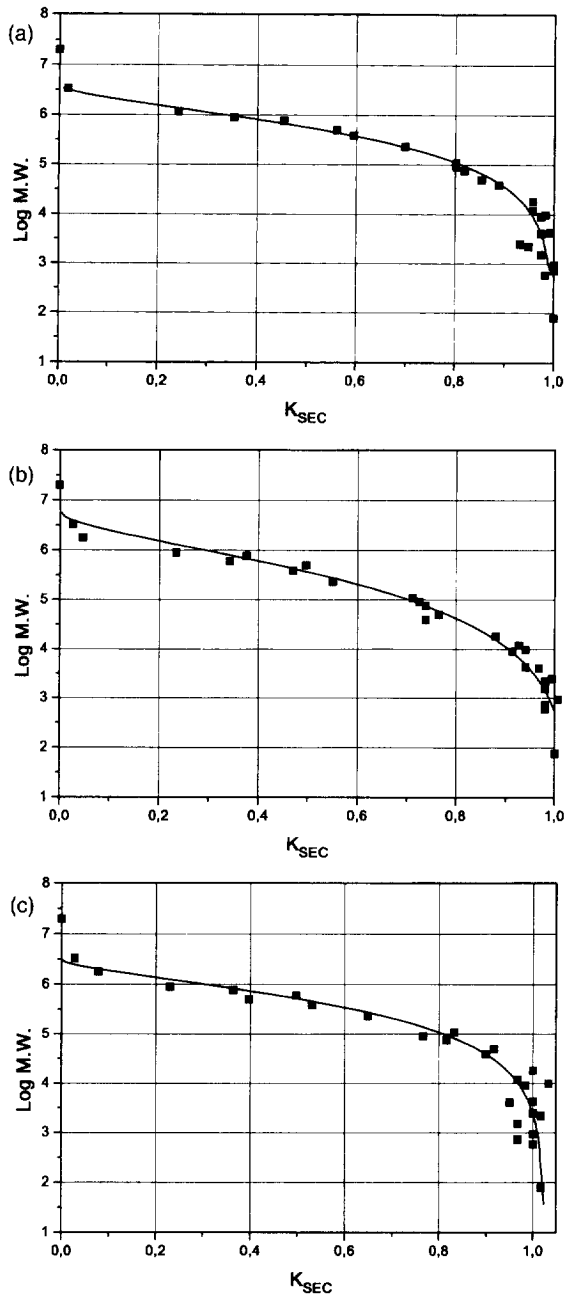

Fig. 4. SEC-curves of MEM-packings. (a) MEM-200; (b) MEM-100 and (c) MEM-20.

the MEM-200 sample in our experiment. The different porosities of the large pore layers of MEM-20 and MEM-200 are also evident viewing Fig. 1c and Fig. 2c. It appears from Fig. 1c and Fig. 2c, that the pore walls of MEM-20 material are markedly thicker then the pore walls of MEM-200 material.

The specific pore volume of 0.544 ml/g of the MEM-100 material was larger than that of the MEM-200 material (0.493 ml/g, Table 2). Therefore, it is reasonable to attribute the difference of 0.052 ml/g to the porosity of the layer composed of 100 nm pores. It should be added that mercury porosimetry was not able to discriminate between the two types of pores in the MEM-100 material, which were clearly identified by SEM. Only one sharp step exists in the intrusion curve (Fig. 3b) which looks very similar to the intrusion curve obtained for the symmetrical MEM-200 membrane (Fig. 3a). The mean pore diameter calculated for the MEM-100 membrane from mercury porosimetry was even slightly higher (Table 2) than the mean pore diameter of the MEM-200 material. Therefore, neither mercury porosimetry nor the low temperature nitrogen sorption were able to provide correct information on the porosity of the packings studied. A reliable measure was only obtained by combination of both methods with scanning electron microscopy.

The pore size distribution of MCM-41, calculated according to BJH method from low temperature nitrogen sorption, revealed a narrow pore size distribution of the packing with a mean pore diameter of 4.3 nm. The specific pore volume obtained from adsorption measurements was 0.82 ml/g (Table 1). The mercury porosimetry of MCM-41 revealed a much higher value for the specific pore volume of 2.01 ml/g calculated from the intrusion curve at $p_{max} = 2000$ bar. No discrimination could be made between the inter- and intra-particle pore volume (Fig. 3d). The pores sizes range from 4 nm to almost 10 000 nm. It appears, that the primary pores of 4.3 nm, detected by the nitrogen sorption measurements and by TEM, were not filled by mercury even at the highest pressure provided by the apparatus used ($p_{max} = 2000$ bar) (Fig. 3). The results of mercury porosimetry were confirmed by SEM: with an increase of the magnification no definite particle shape could be observed providing some type of the fractal structure. The structure is composed of agglomerated primary particles of a mean size of ca. 50 nm. The latter have a hexagonal array of pores with a mean pore diameter of 4 nm.

3.2. SEC of polystyrenes

The SEC-calibration curves of MEM packings (Fig. 4) have a common S-shape without any steps, which should be expected as a result of biporous structure of the MEM-100 and the MEM-20 packings. The specific pore volume calculated from SEC measurements coincided fairly well with the specific pore volume determined by mercury intrusion porosimetry (Table 1).

Unexpectedly, two steps in the calibration curve were obtained for MCM-41 (Fig. 5). The first step corresponds to an exclusion limit of molecular mass of about 4000, while the second step is rather broad and does not display an upward part. Therefore, the exclusion limit and the interstitial volume of the column could be determined only approximately. The calibration curve obtained can be interpreted on the basis of the bimodal pore structure of the MCM-41 material in the column. The first step reflects the porosity of the primary particles, while the second one relates to the porosity of aggregates formed from primary particles and to the interparticle volume. The specific pore volume of MCM-41 calculated from SEC-calibration curve is three times lower than it was found by mercury porosimetry, but coincides fairly well with the specific pore volume measured by the low temperature nitrogen sorption (Table 1). Nevertheless, one should recognize that the coincidence of the results of the last two methods is only apparent. The pore size distribution calculated from the nitrogen desorption isotherm gave no indication of any additional porosity in the MCM-41 structure and the total specific pore volume of 0.82 ml/g thus can be considered as the volume of the pores of primary particles. The SEC-calibration curve gives evidence of two types of pores in the MCM-41 material. The first type represents the mesopores of the primary particles, the second the pores of the aggregates formed by the assembly of the primary particles. The specific pore volume of mesopores of the primary particles calculated from the first step is about 0.47 ml/g. This value is only half of the value determined by the nitrogen sorption measurement. The residual volume of 0.47 ml/g is a sum of the pore volume of the aggregates and the volume between the particles. It is approximately four times smaller than the specific pore volume measured by mercury porosimetry. As mentioned above, the specific pore volume obtained by mercury porosimetry is equivalent to the intra-particle pore volume, but does not include the volume of the 4 nm pores of the primary particles. Therefore, the difference between the intra-particle volume measured by SEC and the volume measured by mercury porosimetry is self-explaining: the highest-molecular-mass polymer used is too small to account for the whole inter- and intra-particle pore volume. Summarizing the results, one can conclude that non of the three methods applied for the assessment of porosity of MCM-41 was able to provide a reliable information and it seems that the pore structure of MCM-41 is more complex than it is commonly discussed.

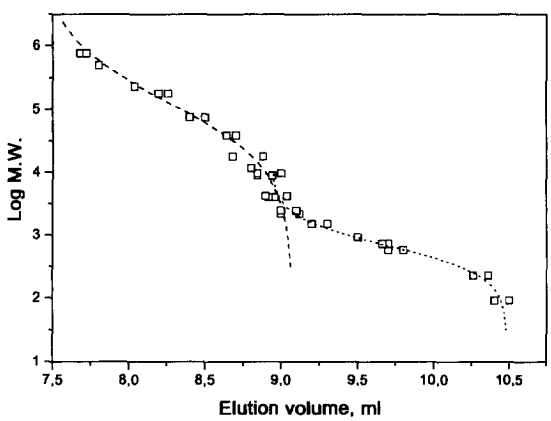

Fig. 5. SEC-curve of MCM-41 packing.

4. Discussion

4.1. Anatop membrane packing MEM-200

The MEM-200 packing possesses throughgoing cylindrical pores without any intersections. Thus, the mercury porosimetry gives the real value of a mean pore diameter (Table 1) and Eq. (3) with $\lambda=2$ should account for the experimental values of K_{SEC} when a correct value of molecular radius of polystyrene is applied. In all definitions of the dimension of a polymeric molecule the radius is correlated to the molecular mass of the polymer though the equations similar to the Mark–Houwink equation,

i.e. $r=aM^b$ (see Section 2.5). To obtain the best fit of the experimental data, the relation was used in Eq. (3) with a variation of the coefficients a and b. The fitting of the experimental points is shown in Fig. 6 and the values of $a=0.080$ and $b=0.630$ were obtained. The corresponding radius is designated according to Degoulet [29] as a chromatographic radius r_C and deviates markedly from the Stokes radius, the hydrodynamic radius and the radius of gyration (Eqs. (4,5,7)). Thus, the fit of the experimental data by Eq. (1) with the Stokes radius or with the hydrodynamic radius significantly overestimates the experimental values (Fig. 6). Unexpectedly, only minor differences were observed between the fitting curves obtained with r_C and with r_g (Fig. 6). Closer analysis of the fitting procedure revealed that the coefficients a and b correlate strongly with each other. Thus, an increase in the values of a caused a corresponding decrease in the values of b in such a way that χ^2 values remain constant within an error of $\pm 10\%$. The interval of corresponding values of a ranges from 0.14 to 0.05 and of b ranges from 0.59 to 0.67. The coefficients in Eq. (5) are within these intervals and correlate well with each other. As a result only minor differences were observed in the corresponding fitting curves (corresponding χ^2 values are $5.0\cdot10^{-4}$ and $5.9\cdot10^{-4}$, respectively). The coefficients a and b of the Stokes radius (Eq. (4)) and the hydrodynamic radius (Eq. (5)) are not within these intervals and thus, they do not correlate with each other. As a result the corresponding fitting curves deviate markedly from the experimental data.

The Eq. (3) fits fairly well the experimental points over the whole range of molecular masses studied except the highest ones. This can be a result of the approximations made in the model, i.e., the assumptions of hard spheres for polymeric molecule and the uniform pore structure of the packings. A theoretical treatment of flexible polymeric chains in equally sized cylindrical pores was addressed by Casassa [10]. He derived the following expression for the distribution coefficient:

$$K = 4\sum_{m=1}^{\infty} \beta_m^{-2} \exp([-\beta_m^2(<s^2>/R^2)] \qquad (8)$$

where $<s^2>$ is the mean square radius of gyration of polymeric molecule, R is the radius of the cylindrical pore and β_m are roots of the equation $J_0(\beta)=0$ (J_0 is the Bessel function of the first kind of order zero). Fitting of experimental points by Eq. (8) is shown in Fig. 7. Again, the Eq. (8) overestimated the distribution coefficient K, when the Stokes radius r_S is used. Only very small difference was observed in the fitting curves calculated with r_g according to Eq. (7) and with r_c obtained as it is described above. These plots fitted fairly well the experimental points in the range of low and high

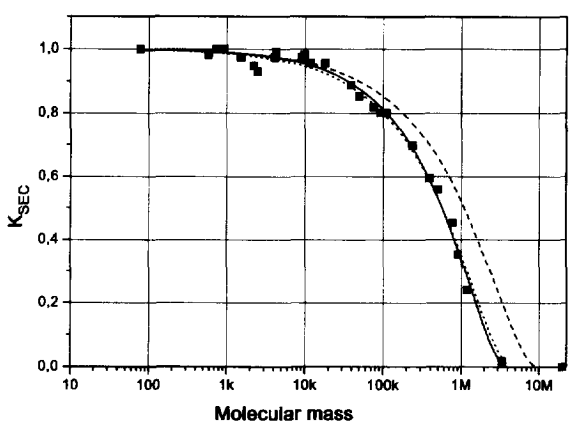

Fig. 6. Fitting the experimentals point of SEC-curve of MEM-200 packing with Casassa's models [8] (solid line – the best fit of Eq. (1), dotted line – Eq. (1) with the radius of gyration, dashed line – Eq. (1) with the Stokes radius).

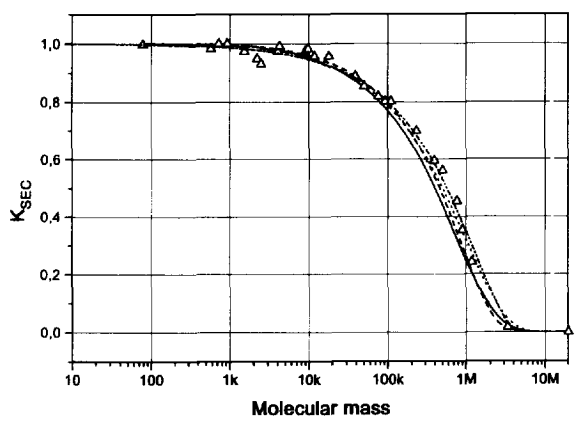

Fig. 7. Comparison of Casassa's [10] and Dubin's [18] models on the fitting of the experimental points of SEC-curve of MCM-41 packing (dashed line – Casassa's model Eq. (8), dotted line – Dubin's model Eq. (7), dashed-dotted line – the best fit of Eq. (1), solid line – calculated with Yau's model [28]).

values of the distribution coefficient. Some discrepancy still remains in the range of K between 0.2 and 0.6. That may be due to the finite pore size distribution of pore radius of packing, which is not accounted by Casassa's model.

The pore size distribution of packing was incorporated in Eq. (3) assuming cylindrical pores and Gaussian pore size distribution by Dubin et al. [18] and gave the following equation:

$$K = \left[\frac{\sqrt{\pi}}{2}\left(1 - erf - \frac{\bar{R}}{\Delta R}\right) \right]^{-1} \times \int_{r}^{\infty} (1 - \frac{r}{R})^2 \exp\left[- \frac{(R - \bar{R})^2}{\Delta R^2} \right] dR \qquad (9)$$

where R is the mean pore radius, ΔR is the width of the pore size distribution and r is the radius of the polymeric molecule. Because the pore size distribution of MEM-200 does not follow a Gaussian distribution, the Eq. (9) was modified in such a way that the pore size distribution obtained from mercury porosimetry was implemented. The fitting of the experimental points by the modified Eq. (9) with the molecular dimensions of the polymeric molecule taken as chromatographic radius is shown in Fig. 7. Comparing Casassa's model with the model of Dubin (Fig. 7) one can see, that both models underestimated the experimental data in the range of K between 0.8 and 0.4. Above and below this range Casassa's model gave a better fit of the experimental results, but the difference between the models is relatively small. To obtain a better fit of the experimental points in the middle range of the distribution coefficient we tried to combine both theories in the same manner as was done by Dubin [18] for Ackers theory [11]. Instead of geometrical weighting by Eq. (3) in Dubin's model (7) we applied a weighting given by Casassa's function (8). This model was suggested by Yau et al. [28]. Unfortunately, the fitting with this model did not give any improvement in the description of the experimental data. The fitting in the middle range of the distribution coefficients was even poorer than by Casassa's model (Fig. 7). Therefore, we used Casassa's model [10] in the treatment of the experimental data of other packings in the study, because it gave the best fit of the experimental points.

4.2. MCM-41 packing

MCM-41 packings can be considered as an ideal packing to be described with Casassa's function because its primary pores are an array of uniform hexagonal cylinders. Unfortunately, the subsequent agglomeration of the primary particles formed a secondary pore structure, which is not well separated in the SEC-calibration curve from the mesopores of the primary particles (Fig. 5). We resolved both regions in the SEC-curve by a fitting program taken two sigmoidal functions into account (Fig. 5). Furthermore, the experimental points within the region of primary pores were fitted by Casassa's function (Eq. (6)) using the chromatographic radius r_c of polystyrenes obtained for the MEM-200 material. MEM-200 has a mean pore size of 200 nm and the chromatographic radius obtained relates to the polystyrene molecules with a molecular mass between 10^6 and $5 \cdot 10^3$. Due to the small pore size of MCM-41 solutes of a molecular mass smaller than 5000 can only penetrate the pores of the primary particles. The molecular dimensions of low-molecular-mass polystyrenes might deviate from those calculated with equation $r = 0.08M^{0.63}$ obtained for the high-molecular-mass polystyrenes. The variation of the coefficients in the Eqs. (4–7) over a wide range of molecular masses is well known in polymer chemistry (see for example [36]). Nevertheless, as it can be seen in Fig. 8, Casassa's model provides a good fit of the experimental points up to a molecular mass of ca. 500. Marked differences are observed only in the range of molecular masses smaller than 500. This discrepancy can be expected due to some inconsistency between the theory and the experimental measurements. Knox and Scott [22] pointed out that the total pore volume of any packing can be only estimated with a probe molecule of indefinitely small size. The real probe molecule (toluene in this study) has always a finite size and therefore, some corrections of the pore volume obtained is needed. In contrast to Knox and Scott, Waldmann-Mayer [17] supposed that small molecules can penetrate at some extent even the skeleton of the packing. As a consequence, the measured distribution coefficient will become larger than given by Eq. (1). The corrected expression according to Waldmann-Mayer is:

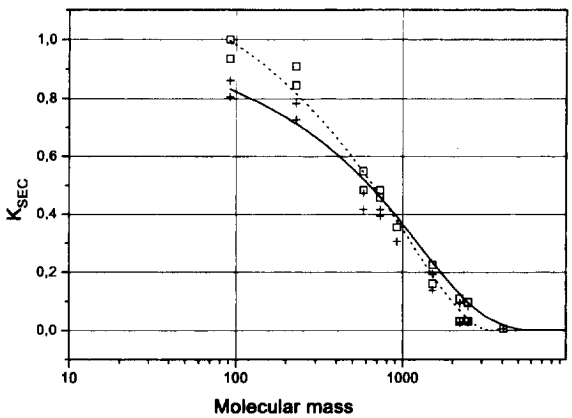

Fig. 8. Fit of the experimental points of SEC-curve of MCM-41 packing with Casassa's model (Eq. (8)). (solid line – calculated with Casassa's model without corrections, □ – experimental points, + – experimental points corrected according to Knox [22], dashed line – calculated according to Waldmann-Mayer [17]).

$$K=\left(A-\frac{r}{R}\right)^{\lambda}=\left(A-\frac{aM^{b}}{R}\right)^{\lambda} \qquad (10)$$

where A is the ratio $(R+\delta)/R$ (δ is the thickness of the intravitreous penetration layer). The model of Waldmann-Mayer seems to be somewhat doubtful, particularly for rigid inorganic particles. When the experimental points of SEC-calibration curve of the MEM-200 packing have been fitted by the Eq. (10), the following values of the coefficients of Eq. (10) were obtained: $A=0.998$, $a=0.07$ and $b=0.64$ with $\chi^2=5.0\cdot10^{-4}$. Hence, the same values of the chromatographic radius were obtained and no penetration could be detected (A is close to 1). Nevertheless, considering that MEM-200 is a wide pore material, both models were tested to improve the fit of the experimental points of MCM-41 packing.

An increase of the total pore volume by a factor of 1.024 according to Knox and Scott brought the measured values of the distribution coefficients in a fairly good agreement with Casassa's fitting plot (Fig. 8). The correction factor 1.024 was even smaller than the one used by Knox (1.087) [22].

To obtain a reasonable fit with Waldmann-Mayer's model one has to vary all coefficients in Eq. (9). Under these circumstances an excellent agreement with the experimental points was obtained (Fig. 8). The value of coefficient A (1.127) reveals that the thickness of the penetration layer is about 2.5 Å and the chromatographic radius had to be changed to $r_c=0.172M^{0.598}$ as compared with $r_c=0.08M^{0.63}$ found for the high-molecular-mass polystyrenes. All the coefficients of the model by Knox and by Waldmann-Mayer gave reasonable values. Therefore we cannot distinguish between the two models. The value of the pore diameter of 4 nm of the primary pores in MCM-41 could be estimated with both models.

4.3. MEM-100 and MEM-20 packings

The asymmetrical membrane packings MEM-100 and MEM-20 provide two types of cylindrical throughgoing channels in their structure as detected by means of SEC and mercury porosimetry. The investigations of MEM-100 and MEM-20 packings have been performed to elucidate the resolving ability of the ISEC technique.

The SEC-calibration curves of MEM-100 and MEM-20 packings have a very similar S-shape form without any indications to the bimodal pore structure (Fig. 4). However, the fit of the experimental points by Casassa's Eq. (8) with the chromatographic radius of polystyrene gave a fairly good fit over the whole range of molecular masses for MEM-20 material, assuming a mean pore radius of 115 nm (Fig. 9). Under the same circumstances Casassa's model fitted reasonably well only the high-molecu-

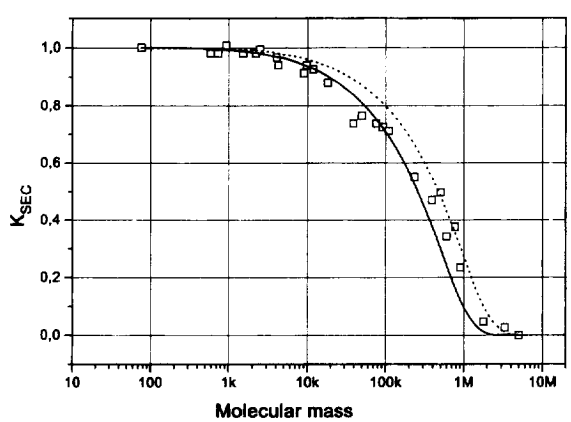

Fig. 9. Fitting the experimental points of SEC-curve of MEM-100 packings with Casassa's model (Eq. (8)) (solid line with mean pore radius of 80 nm, dashed line with mean pore radius of 115 nm).

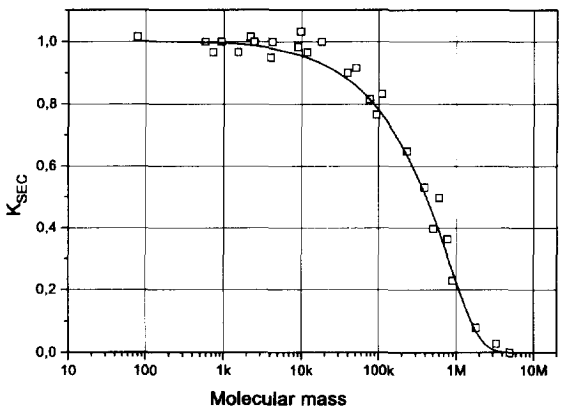

Fig. 10. Fitting the experimental points of SEC-curve of MEM-20 packing with Casassa's model (Eq. (8)).

lar-mass range of SEC-curve of MEM-100 packing. In the low-molecular-mass range the computed curve overestimated the experimental values (Fig. 10). When the mean pore radius of the packing was taken as 80 nm, a good fitting was obtained for the low-molecular-mass range, but the high-molecular-mass range was underestimated. It appears that, in terms of Casassa's model, the MEM-100 packing has to be considered as a packing with a bimodal pore size distribution. The separation of the two regions can be hardly made without a fitting of the experimental points by a theoretical model because both regions almost merged into each other. Therefore, the analysis of the SEC-calibration curve could provide some indication of the biporous structure of the MEM-100 packing which could not be obtained from mercury porosimetry. There was no indication of a biporous structure of the MEM-20 packing, which was clearly observed at the mercury intrusion curve. It can be attributed to the rather small pore volume of MEM-20 of 0.20 ml/g, which could not be measured by SEC with significantly high accuracy.

5. Conclusion

For the first time SEC of polystyrenes has been performed on the MEM-200 packing. Its pore structure fits to all assumptions made on the determination of its porosity by mercury porosimetry. This allowed to test the application of different theoretical models in SEC to describe the experimental data obtained with the MEM-200 packing. Good results were achieved with the classical model of Casassa [10], derived for polymeric solutes with a flexible polymeric chain, while other models in spite of their complexity did not provide significant improvement in description of the experimental data.

The chromatographic radius of polystyrene solutes obtained by fitting the experimental points with Eq. (3) coincided with none of the common radii of polymeric molecules used in polymeric chemistry. Nevertheless, the fitting curve calculated with the radius of gyration differed only slightly from the fitting curve using the chromatographic radius. It appears that the chromatographic behavior of polymers can be approximated best of all by the radius of gyration, when the chromatographic radius is not known. The use of the Stokes radius or the hydrodynamic radius led to fitting curves which markedly overestimated the experimental data.

Neither SEC nor mercury porosimetry alone were able to describe correctly the bimodal pore structure of the MEM-100 and MEM-20 packings. The results obtained from the analysis of the SEC measurements and from mercury porosimetry complemented each other and provided a good basis for the relevant evaluation of the porosity of these packings.

Casassa's model described reasonably well the SEC behaviour of MCM-41 packing with the chromatographic radius of polystyrenes obtained with the MEM-200 packing. A correction was only needed in the range of the smallest molecular masses and can be easily made according to Knox [22] or Waldmann-Mayer [17]. The chromatographic behaviour of MCM-41 is indicative for the cylindrical pore shape of the packing demonstrating the sensitivity of SEC calibration curve with respect to the pore shape.

Acknowledgments

The authors are grateful to Dr. Jones (Whatman, Bunbury, UK) for a gift of research samples of Anatop membranes and to Mr. Lubda (E. Merck, Darmstadt, Germany) for the assistance in the measurements of porosity of packings, by means of mercury porosimetry.

References

[1] H.G. Barth, B.E. Boyes and C. Jackson, Anal. Chem., 66 (1994) 595R.
[2] L.Z. Vilenchik, J. Asrar, R.C. Ayotte, L. Ternorutsky and C.J. Hardimann, J. Chromatogr., 648 (1993) 9.
[3] T.C.Laurent, I. Bjork, A. Pietruszieklewitz, H. Persson, Biochim. Biophys. Acta, 83 (1963) 351.
[4] T.C. Laurent, H. Persson, Biochim. Biophys. Acta, 84 (1964) 351.
[5] T.C. Laurent, J. Klander, J. Chromatogr., 14 (1964) 317.
[6] J. Porath, Pure Appl. Chem., 6 (1963) 233.
[7] V. Grubisic, P. Rempp and H. Benoit, J. Polym. Sci., B 5 (1967) 753.
[8] E.F. Casassa and Y. Tagami, Macromolecules, 2 (1969) 14.
[9] C.J. Giddings, E. Kucera, C.P. Russell and M.N. Meyers, J. Phys. Chem., 72 (1968) 397.
[10] E.F. Casassa, J. Phys. Chem., 75 (1971) 275; J. Polym. Sci., Part B, 5 (1967) 773.
[11] G.K. Ackers, J. Biol. Chem., 242 (1967) 3237; Adv. Protein Chem., 24 (1970) 343.
[12] M. Van Kreveld and N. Van den Hoed, J. Chromatogr., 83 (1973) 111.
[13] W.W. Fish, Methods Membr. Biol., 4 (1975) 189.
[14] K. Horiike, H. Tojo, M. Iwaki, T. Yamano and M. Nozaki, Biochem. Int., 4 (1982) 477.
[15] K. Horiike, H. Tojo, Y. Yamano and M. Nozaki, J. Biochem. (Tokio), 93 (1983) 99.
[16] L.C. Davis, J. Chromatogr. Sci., 14 (1983) 214.
[17] H. Waldmann-Mayer, J. Chromatogr., 350 (1985) 1.
[18] S. Hussain, M.S. Mehta, J.I. Kaplan and P.L. Dubin, Anal. Chem., 63 (1991) 1132.
[19] I. Halasz, Ber. Bunsenges. Phys. Chem., 79 (1975) 731.
[20] D.H. Freeman and I.C. Poinescu, Analyt. Chem., 49 (1977) 1183.
[21] B.G. Belenkii and L.Z. Vilenchik, Modern Liquid Chromatography of Macromolecules, Elsevier, Amsterdam, 1983.
[22] J.H. Knox and H.P. Scott, J. Chromatogr., 316 (1984) 311.
[23] K. Jerabek, Anal.Chem., 57 (1985) 1595.
[24] W. Haller, Nature, 206 (1965) 231.
[25] J.J. Kirkland, J. Chromatogr., 125 (1976) 231.
[26] O. Mikes, D. Strop and J. Coupek, J. Cromatogr., 153 (1978) 23.
[27] Y. Kato, T. Kitamura and T. Hashimoto, J. Chromatogr., 333 (1985) 93.
[28] W.W. Yau, C.R. Ginnard and J.J. Kirkland, J. Chromatogr., 149 (1978) 465.
[29] C. Degoulet, J.-P. Busnel and J.-F. Tassin, Polymer, 35 (1994) 1957.
[30] F. Cabre, E.I. Canela and M.A. Canela, J. Chromatogr., 472 (1989) 347.
[31] C.T. Kresge, M.E. Leonovich, M.E. Roth, J.C. Vartuli and J.S. Beck, Nature, 359 (1992) 710.
[32] A. Kurganov, U. Ciesla, St. Schacht, F. Schüth and K. Unger, Presented at the 5th International Conference on the Fundamentals of Adsorption, Asilomar, Pacific Grove, California, May 13–18, 1995.
[33] Polymer Handbook, J. Brandrup and E. Immergut (Editors), J. Wiley and Sons, New York, 1989, pp. VII/15 and VII/38.
[34] C. Tanford, Y. Nozaki, J.A. Reynolds and S. Makino, Biochemistry, 13 (1984) 2369.
[35] R.E. Martenson, J. Biol. Chem., (1978) 8887.
[36] R.A. Sanayei, S. Pang and A. Rudin, Polymer, 34 (1993) 2320.